Exploring the cation dynamics in lead-bromide hybrid perovskites

Carlo Motta,[1,*] Fedwa El-Mellouhi,[2] and Stefano Sanvito[1]
[1]*School of Physics, AMBER and CRANN Institute, Trinity College, Dublin 2, Ireland*
[2]*Qatar Environment and Energy Research Institute, Hamad Bin Khalifa University, Doha, Qatar*
(Received 31 December 2015; revised manuscript received 23 March 2016; published 8 June 2016)

Density functional theory including a many-body treatment of dispersive forces is used to describe the interplay between structure and electronic properties of two prototypical Br-based hybrid perovskites, namely, $CH_3NH_3PbBr_3$ and $HC(NH_2)_2PbBr_3$. We find that, like for some of their iodine-based counterparts, the molecules' orientation plays a crucial role in determining the shape of both the conduction and valence bands around the band edges. This is mostly evident in the case of $CH_3NH_3PbBr_3$, which is a direct band-gap semiconductor when the CH_3NH_3 group is oriented along the (111) direction but turns indirect when the orientation is (100). We have constructed a simple dipole model, with parameters all evaluated from *ab initio* calculations, to describe the molecules' depolarization dynamics. We find that, once the molecules are initially orientated along a given high-symmetry direction, their room-temperature depolarization depends on the specific material investigated. In particular we find that the ratio between the polarization decay constant of $CH_3NH_3PbBr_3$ and that of $HC(NH_2)_2PbBr_3$ is about 2 at room temperature. With these results at hand we suggest a simple luminescence decay experiment to prove our findings and establish a correlation between optical activity and the molecules' dynamics in these materials.

DOI: 10.1103/PhysRevB.93.235412

I. INTRODUCTION

Hybrid organic-inorganic perovskites, such as the prototypical methylammonium lead iodine $CH_3NH_3PbI_3$, have recently taken materials science by storm. In fact, in the last 3 years they have demonstrated an unprecedented portfolio of successes in applications such as efficient and affordable solar cells [1–5], optoelectronics and lasing devices [6–9], sensors [10,11], and tandem solar electrochemical water-splitting cells [12], just to name few. The quest for high photovoltaic efficiencies combined with solid structural stability, cheap fabrication processes, and, most importantly, environmentally friendly chemical compositions [13] have motivated the development of sophisticated synthesis and preparation strategies for this class of materials. Synthesis includes halide replacement and mixing, the search for Pb substituents, and alternative cation molecules. As a consequence of the effort for modifying $CH_3NH_3PbI_3$, considerable activity has been devoted to develop Br-based perovskites. Such effort has been successful, and in 2014 a power-conversion efficiency of more than 10% has been reported [14] for solar cells made of methylammonium lead bromide, $CH_3NH_3PbBr_3$ ($MAPbBr_3$). Subsequently, high-performing solid-state solar cells based on $MAPbBr_3$ quantum dots with an 11.4% efficiency and cell lifetimes of more than 4 months have also been reported [15]. Finally, nanoparticles of these Br-based perovskites have been recently proposed as a new material for light-emitting diodes [16], and their application as visible-light emitters was also demonstrated [7].

Interestingly, methylammonium is not the only cation that can be incorporated into the $XPbBr_3$ perovskite structure. Hanusch *et al.* reported highly efficient wide-band-gap planar heterojunction solar cells based on the structurally related formamidinium lead bromide, $HC(NH_2)_2PbBr_3$ ($FAPbBr_3$). They showed that in this material the photoexcited species have diffusion lengths longer than those of their methylammonium counterpart. This results in planar heterojunction solar cells exhibiting power-conversion efficiencies approaching 7%, with good prospects for using $FAPbBr_3$ in solar cells with wide-band-gap absorbers [17]. As predicted, $FAPbI_3$-based perovskite solar cells with maximum power-conversion efficiency greater than 20% have been recently reported [18], and bromide hybrid perovskites have been also employed for sensor applications [11].

An important feature of both $MAPbBr_3$ and $FAPbBr_3$ is that they can be synthesized in high-quality macroscopic single crystals. Interestingly, a study on point defects in $MAPbBr_3$ [19] showed that the materials' performances are highly tolerant to defect formation, suggesting that stable defects may induce shallow levels in the band gap. Kunugita *et al.* [20] recently investigated the excitonic properties of these compounds as a function of temperature. The study revealed that electron-hole pairs remain bound even at room temperature. They estimated that the exciton binding energy ranges between 80 and 100 meV and remains unchanged upon a temperature increase and structural phase transition. In this study the photoluminescence line broadening with temperature was attributed to exciton-phonon interaction. An evaluation of the coupling between the exciton and the longitudinal optical (LO) phonon [20] resulted in the frequency of the LO phonon being estimated to be $\omega_{LO} = 16.8 \pm 2.4$ meV (135 ± 20 cm^{-1}). Hence, it appears that the dynamic of the MA and FA molecules crucially impacts the optical and electronic properties of this class of materials.

Here we investigate the dynamics of MA and FA molecules within the perovskite lattice and suggest a simple photoluminescence anisotropy decay experiment as a tool to correlate such dynamics with the optical activity. In our opinion this is, at present, the missing information for understanding the optical behavior of such a fascinating class of materials. In fact, although there is rich literature on both the molecules'

*mottac@tcd.ie

dynamics and their light-absorbing properties, no direct connection between the two aspects has ever been made. Thus, we construct here a simple dipolar model with parameters extracted from accurate electronic structure theory, which we use to extract the time-decay constants of the various molecular species at finite temperature. The model suggests that the time relaxation is rather different in $MAPbBr_3$ and $FAPbBr_3$, with the differences being robust against temperature.

This paper is organized as follows. In the next section we describe our computational method and provide details of the calculations. Next, we examine the structural, electronic and dynamical properties of the two compounds and construct a simple dipolar model. This is solved by Monte Carlo simulations at finite temperature. Finally, we conclude.

II. COMPUTATIONAL DETAILS

Structural optimization is performed by density functional theory (DFT), where the exchange and correlation energy is calculated at the level of the generalized gradient approximation (GGA) with the Perdew-Burke-Ernzerhof (PBE) [21] parametrization. In particular we have employed the all-electron FHI-AIMS code [22]. Long-range van der Waals interactions are taken into account and are computed at different levels of approximation, namely, the pairwise Tkatchenko-Scheffler (TS) scheme [23] and the many-body dispersion (MBD) approach [24]. These are both implemented together with the GGA. The reciprocal space integration is performed over an $8 \times 8 \times 8$ Monkhorst-Pack grid [25]. A preconstructed high-accuracy all-electron basis set of numerical atomic orbitals is employed, as provided by the FHI-AIMS "tight" default option. The geometry relaxation is performed with the Broyden-Fletcher-Goldfarb-Shanno algorithm [26], where both the internal coordinates and the supercell lattice vectors are optimized until the residual force is smaller than 10^{-3} eV/Å . The atomic zeroth-order regular approximation is also applied to treat relativistic effects. When needed, perturbative spin-orbit coupling [27] is included to compute the band structure.

The phonon spectra at the Γ point have been computed with the frozen-phonon approach by using the PHONOPY [28] package in combination with the dynamics matrix evaluated from DFT and van der Waals interaction with FHI-AIMS. This is effectively a finite-difference method, and a displacement of 0.001 Å has been applied to each atom in the three space directions to compute the dynamical matrix. The minimum energy paths associated with the molecular rotations have been obtained by using the string method [29] as implemented in AIMSCHAIN. The climbing image feature [30] has been used with six images and a tight convergence of 0.05 eV/Å.

III. RESULTS AND DISCUSSION

A. Structural properties

We have chosen to investigate Br-based hybrid perovskites since they crystallize in a highly symmetrical cubic structure for both the MA and FA cations [17]. The *Pm3m* symmetry group exhibits no octahedral rotation or tilts, enabling us to single out the effects of the dynamical motion of the molecules from that of the $PbBr_6$ octahedral framework that would otherwise influence the band structure and the phonon frequencies. The crystal geometries of $MAPbBr_3$ and $FAPbBr_3$ have been optimized by our all-electron DFT calculations starting from the x-ray diffraction refined atomic positions [17]. Recent nuclear magnetic resonance experiments suggest a disordered arrangement of the MA group and a highly anisotropic displacement of the Br atoms around ellipsoids centered at their equilibrium position [31]. Thus, we have performed several structural relaxations with different initial orientations of the MA and FA cations parallel to all symmetry axes and for different rotations around them. Our calculations indicate that FA displays only one energy minimum oriented parallel to the (001) axis, while MA displays two stable configurations, namely, along the cubic cell axes (001) (global minimum) and along the diagonal (111) as demonstrated in the case of lead iodide perovskites [32,33].

The optimized structures are in excellent agreement with the experimental x-ray diffraction data [17] only when van der Waals interactions are considered. In particular, the best agreement is achieved by the MBD correction scheme [24]. In fact, PBE overestimates the equilibrium volume by 6.5% for FA and by 2.3% and 8.65%, respectively, for MA for the (001) and (111) orientations. The same quantities are overestimated by 0.9%, 7.2%, and 3.2% when the calculation is done with the TS method and by 1.5%, 2.9%, and 3.9% for the MBD scheme. The resulting MBD-optimized geometries for the FA and MA(001) structures are shown in Fig. 1, where the hydrogen bonds have been explicitly represented by calculating the noncovalent interaction (NCI) densities [34]. For $FAPbBr_3$ the NCI density describes four hydrogen bonds being formed between the H atoms of the ammonium moiety and the neighboring Br ions. In the case of MA, the same hydrogen atoms form three hydrogen bonds in both the (001) and (111) configurations [35]. We find that the four H-Br bonds in FA are much shorter (2.49–2.51 Å) than the ones formed by MA (3.1–3.3 Å), even though the volume of the $FAPbBr_3$ unit cell is larger than that of $MAPbBr_3$. This suggests that the molecular motion of FA is more restricted due to the large confinement evidenced by the shorter Br-H bonds, which in turn suggests stronger inertia to rotation. Interestingly, the

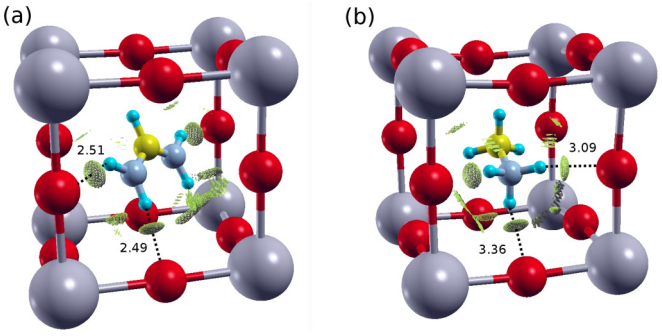

FIG. 1. Optimized structures for the *Pm3m* phase of (a) $FAPbBr_3$ and (b) $MAPbBr_3$. The dotted lines indicate the hydrogen bonds between H and Br, and the bond lengths are in angstroms. The noncovalent interaction density isosurfaces, shown in green, provide a useful representation of the hydrogen bonds occurring between the H and Br atoms.

symmetry-equivalent molecular orientations are governed by the couplet/triplet of hydrogen bonds bearing excess positive charge forming with Br.

B. Electronic properties

We now analyze the electronic properties of the two compounds calculated for the optimized structures. The choice of cation has some impact on the materials' electronic band structure. When one uses the PBE functional the band gap is calculated to be 1.84 eV for $FAPbBr_3$, 1.96 eV for $MAPbBr_3$ when MA is oriented along (001), and 1.89 eV when MA is along (111). These values are significantly smaller than the reported experimental ones of 2.2 eV and 2.35 eV for $FAPbBr_3$ and $MAPbBr_3$, respectively. A treatment of the exchange and correlation functional going beyond local and semilocal approximations, such as that provided by the Heyd-Scuseria-Ernzerhof hybrid functional HSE06 [36], significantly improves the description and returns the following band gaps: 2.38 eV for $FAPbBr_3$, 2.53 eV for $MAPbBr_3$ (001), and 2.42 eV for $MAPbBr_3$ (111). These, however, still need to be corrected for spin-orbit interaction, which is rather strong in the Pb-derived valence band [32]. In any case, regardless of the choice of the functional, all calculations are consistent with the generic trend that associates the MA cation with a larger band gap, in agreement with the experimental observations. As an illustration, in Fig. 2 we present the band structure obtained by PBE including spin-orbit interaction, noting that the HSE06 bands are similar with the exception of a larger band gap.

In general $MAPbBr_3$ and $FAPbBr_3$ present rather similar band structures. A notable difference is a shift of the conduction-band minimum from R in the case of $MAPbBr_3$. The occurrence of Rashba splitting in these materials has been studied extensively in the literature [5,37–42], and it has been shown to be emphasized by uniaxial strain induced by the organic cation [32]. Indeed, for $MAPbI_3$ we observe a strong shift of the conduction-band minimum for the (001) orientation of MA due to the cation-induced strain of the inorganic matrix. Although the same effect can still be noticed in $FAPbBr_3$, it is much less pronounced since the relaxed unit cell remains almost perfectly cubic; hence, the band gap is direct. Note also that the curvature of both the valence and conduction bands depends on the cation and its orientation, a fact that will reflect on the effective mass and, ultimately, the carriers' mobility. Finally, note that the FA molecular states are closer to the optical gap region than those of MA, their signature being the flat bands at around 3.5 and −2 eV (taken from the valence-band top). Overall, we can conclude that there are subtle, but qualitative, differences between the electronic band structures of $MAPbBr_3$ and $FAPbBr_3$, suggesting that the photophysical features of PbBr-based perovskites may likely depend on the specific cation and its orientation within the lattice. As a consequence, one may also expect the cation dynamics to play a role in the optical properties. With the goal of suggesting a simple photoluminescence anisotropy decay experiment correlating optical and structural properties, we now explore how the molecules evolve in time at finite temperature.

C. Phonon spectrum and cation dynamics

Bearing in mind that both MA and FA are polar molecules, our goal is to construct an effective dipolar model to investigate the time evolution of the molecules at finite temperature. The crucial point is to extract the various parameters of the model from our accurate DFT analysis. In particular one requires two key ingredients, namely, the knowledge of the material's phonon spectrum and that of the molecules' rotational energy barriers.

The low-energy portion of the phonon spectra of $MAPbBr_3$ and $FAPbBr_3$, as calculated with PBE and the MBD van der Waals corrections, is shown in Fig. 3 (we are not aware of an experimental measurement of such phonon spectra). We find that phonon modes with frequency lower than 100 cm^{-1}

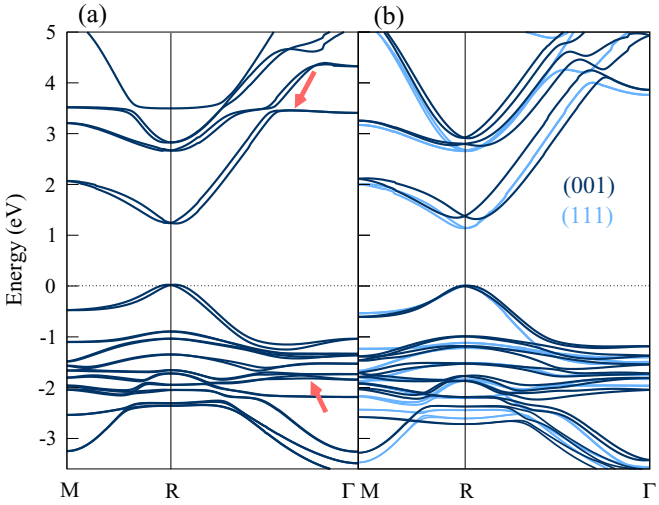

FIG. 2. Electronic band structure of (a) $FAPbBr_3$ and (b) $MAPbBr_3$ calculated at the PBE level and including spin-orbit interaction. In the case of $MAPbBr_3$ we present results for the two inequivalent orientations of the methylammonium cation. The energy zero is taken at the valence band maxima.

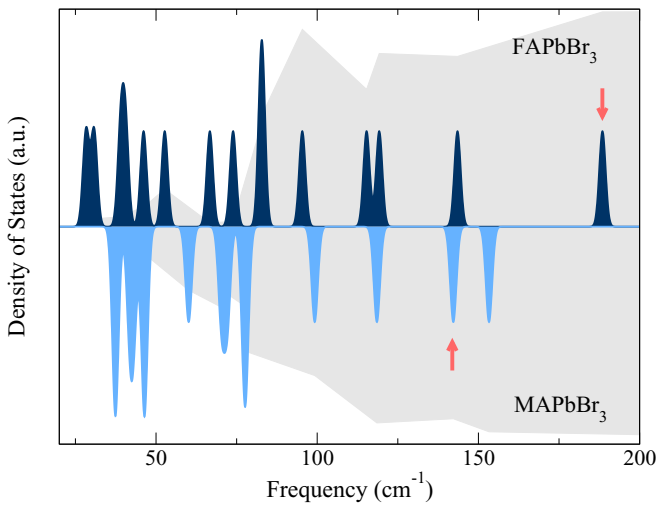

FIG. 3. Phonon density of states at the Γ point for $FAPbBr_3$ and $MAPbBr_3$. The arrows indicate the quasirigid rotational modes of the molecules within the inorganic cage. The shaded area represents the projection of the DOS on the organic molecule on a percentage scale relative to the y-axis range.

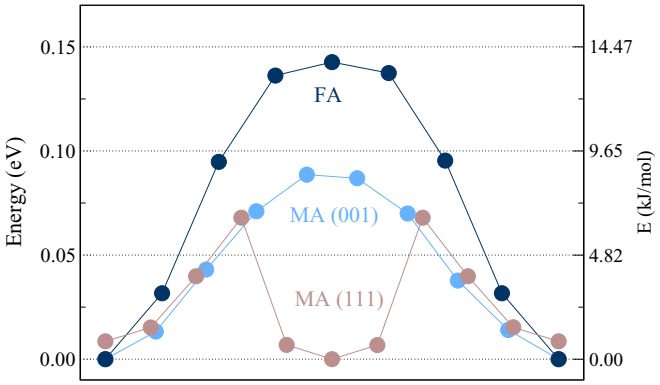

FIG. 4. Calculated potential energy surface associated with a molecular rotation between two stable symmetrically equivalent configurations. The results are shown for FA (blue), MA(001) (cyan), and MA(111) (brown). Note that during the rotation between two (111) directions MA passes through (001) for an angle of 45°.

all correspond to cooperative vibrations of the organic and inorganic sublattices. In contrast, at higher frequencies the molecules librate or vibrate freely, while the $PbBr_6$ cage remains static. By visual inspection of the phonon eigenvectors, we were able to single out modes involving a pure molecular vibration about its rotational pathway that is in the direction of rotation between two equivalent configurations. These modes are found to be at 188 and 142 cm^{-1}, respectively, for FA and MA. Such frequencies translate in attempt times for the rotation of 0.18 ps ($FAPbBr_3$) and 0.23 ps ($MAPbBr_3$). Note that the attempt time is not the time for a full rotation but the average interval between two attempts at a rotation. As such it can be simply estimated from the harmonic frequencies.

We then calculated the minimum-energy path associated with a 90° rotation of the molecules from their ground-state configuration. This essentially means looking at the energy barrier for rotations between two symmetrically equivalent configurations. The potential energy surfaces associated with these paths are shown in Fig. 4. In general the cation rotation induces strain on the $PbBr_3$ sublattice, increasing the total energy. This reaches its maximum when the molecule is rotated by 45°, as it is observable for both FA and MA when rotating from the (001) direction. The case for MA rotating between equivalent (111) orientations is different from the other two because for an angle of 45° the MA molecule is oriented along (001), and thus the rotation path is through the global energy minimum at (001). The energy barriers associated with the rotational processes are summarized in Table I.

From the potential energy surfaces for rotation it appears clear that the FA cation encounters more resistance during the rotation than MA and therefore must display a stronger interaction with the inorganic lattice. This can be attributed to (i) the larger size of the cation and (ii) the nature of the hydrogen bonds. The analysis carried out in Sec. III A shows that the number of H bonds formed between the molecules and the inorganic lattice is larger for FA (four) then for MA (three), stabilizing the structure and thus supporting the bond-counting argument. However, it was also recently argued [35] that the larger dipole moment of MA (2.15 D) with respect to that of FA (0.21 D) should drive a structural stability that is stronger for $MAPbBr_3$ than for $FAPbBr_3$. Although the argument is certainly correct, our structural relaxation returns us a situation in which FA not only is able to form a larger number of H bonds but is also able to keep the bond length significantly shorter (about 25%) than that of the H bonds formed by MA. As such, we conclude that the formation of H bonds is the key interaction driving the stability of the lattice. Further proof of our hypothesis is the fact that the FA rigid rotational frequency is 46 cm^{-1} larger than that of MA.

TABLE I. Rotational energy barriers $K|\mathbf{p}|$ for transitions between high-symmetry configurations of $MAPbBr_3$ and $FAPbBr_3$.

Rotation	$K\|\mathbf{p}\|$ (meV)
FA (001) → (010)	140
MA (001) → (010)	90
MA (111) → (001)	68

With these results at hand, we now construct a classical dipole model to describe the molecules' dynamics within the perovskite lattice at finite temperature. We consider the following Hamiltonian:

$$\hat{H} = \sum_{\langle i,j\rangle_n} \frac{1}{4\pi\epsilon_0}\left(\frac{\mathbf{p}_i\cdot\mathbf{p}_j}{r_{ij}^3} - \frac{3(\hat{n}\cdot\mathbf{p}_i)(\hat{n}\cdot\mathbf{p}_j)}{r_{ij}^3}\right) + K\sum_{i,\alpha=x,y,z}|\mathbf{p}_i\cdot\hat{x}_\alpha| + \sum_i \mathbf{p}_i\cdot\mathbf{E} \quad (1)$$

for an ensemble of three-dimensional dipoles $\{\mathbf{p}_i\}$ of equal magnitude and arranged over a cubic lattice. The first term represents the classical dipole-dipole interaction, which extends over the first n nearest neighbors, where r_{ij} is the distance between the ith and jth dipoles and ϵ_0 is the vacuum permittivity. The second term is an effective potential representing the dipole rotational barrier $K|\mathbf{p}|$. We consider the dipoles with energy minima along the lattice vector directions and a rotational energy barrier of height $K|\mathbf{p}|$, where the different values for FA and MA are assumed to be those calculated for FA and MA(001). Finally, the last term takes into account the presence of a possible external electric field $\mathbf{E}$. The model described by Eq. (1) has been used in the past to investigate the onset of possible ordered ferroic ground states in these materials [43].

The time evolution of the system is investigated by Monte Carlo (MC) simulations using the Metropolis algorithm. At every MC step the lattice dipoles may be updated by choosing a random three-dimensional vector from a uniform spherical distribution. We consider a cubic lattice of $20\times20\times20$ dipoles, where the range of interaction is limited to spheres with a three-lattice-unit radius. The simulations are carried out with periodic boundary conditions. Keeping in mind our goal of proposing a photoluminescence anisotropy decay experiment, we study the depolarization of the dipole network as a function of time. We initialize the system in one ferroelectric configuration with all the dipoles pointing either along the (111) or the (001) direction. Then, in order to determine the depolarization time, the total polarization vector is calculated at every MC step. Note, however, that the Monte Carlo time in

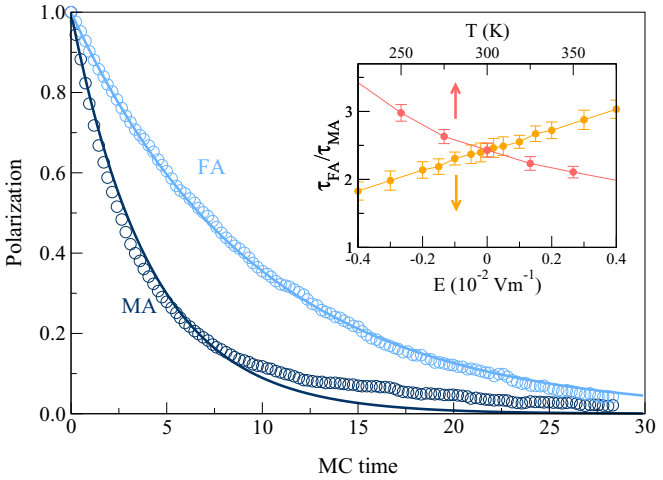

FIG. 5. Total polarization as a function of the rescaled MC time for $FAPbBr_3$ (cyan) and $MAPbBr_3$ (blue) resulting from a Monte Carlo simulation at 300 K of a $20 \times 20 \times 20$ periodic lattice in an initial ferroelectric configuration. Actual data (circles) and the fit function (solid) are shown. In the inset, the ratio τ_{FA}/τ_{MA} is plotted as a function of the temperature (red) and electric field (orange). The data are averaged over 24 simulations, and error bars are shown.

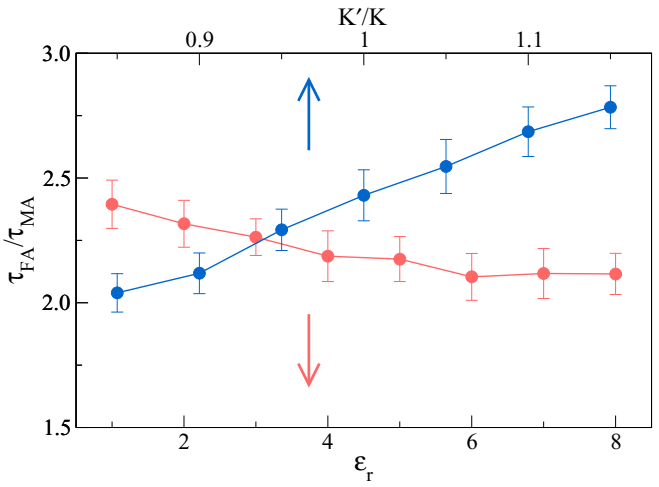

FIG. 6. Dependence of the τ_{FA}/τ_{MA} ratio on some of the model parameters. We present data for a rescaled anisotropy barrier K' and for different permittivity ϵ_r. Note that in both cases the ratio does not change significantly and remains in between 2 and 3. The data are averaged over 24 simulations, and error bars are shown. In both cases simulations are conducted at room temperature.

general cannot be directly associated with the real time since the former depends on the specific MC algorithm chosen, the physical phenomenon being described, and possibly the temperature [44]. Under the reasonable assumption that the MC time is simply linearly proportional to the real time we can then rescale it by the attempt frequencies calculated previously for the rotation phonon modes (for a discussion of this issue see Refs. [44,45]). This will not allow us to extract the absolute value of the dipole relaxation times of MA and FA but to compare the two.

In Fig. 5 we show the calculated time-dependent evolution of the electrical polarization for MA and FA at 300 K (animations of the depolarization process are provided in the Supplemental Material [46]). As expected, FA can hold a macroscopic electrical polarization for longer times with respect to MA, in agreement with our previous considerations that FA interacts with the inorganic sublattice in a stronger way than MA. A fit of the depolarization curves with an exponential function $f(t) = \exp(-t/\tau)$ provides a way to extract the depolarization time τ and returns us a ratio of $\tau_{FA}/\tau_{MA} = 2.3$.

There are a number of assumptions made in our model, and here we test the stability of our results against them. First, we consider the vacuum dielectric permittivity; that is, we assume that the molecules are in vacuum. Recently, it was suggested [47] that the component of the dielectric constant due to the dielectric response of the inorganic lattice (i.e., excluding the molecular contribution) is of the order of 5. We performed MC simulations by varying the permittivity ϵ_r between 1 (the value in vacuum) and 8. Results are shown in Fig. 6 and clearly demonstrate that the ratio between the depolarization times is robust against variations of ϵ_r. Second, our estimate of the rotational barriers K was obtained from DFT calculations for the cubic primitive cell. This can introduce some error since complex atomic relaxations involving more than one cell can effectively reduce such a barrier. In order to account for such error we performed MC calculations in which the effective barrier K is rescaled. Results are presented in Fig. 6 and show that, again, the ratio between the relaxation times of MA- and FA-based perovskites varies by about 30% for changes in K of $\pm 10\%$; that is, it is relatively robust.

Finally, we explore the effects brought by the temperature T and the possible presence of an external electric field. The inset of Fig. 5 shows that τ_{FA}/τ_{MA} (for $\epsilon_r = 1$) decreases as T gets larger, as expected from the fact that a higher temperature cannot distinguish the differences in rotational barriers between the two molecules. However, we note that the interval 250–350 K is the only one where a possible measure can be conducted since below 250 K the materials undergo a structural phase transition, while above 350 K their mechanical stability is seriously compromised. In this range, the time ratio remains in between 2 and 3; that is, it is relatively constant. Finally, we notice that τ_{FA}/τ_{MA} has a weak linear dependence on an eventual external electric field (inset in Fig. 5). Such dependence can be eventually measured under controlled experimental conditions.

If we let the system thermalize in full, by extending the calculations to 10^7 MC steps, we end up in a situation in which the total polarization vanishes. This suggests that at least for this model, there is no ferroic order in the temperature range investigated. However, we observe that the dipole-dipole correlation function as a function of the distance between the dipoles is typically one order of magnitude larger for MA than for FA. Furthermore, by inspecting the thermalized lattices at 300 K, random motifs of three (two) aligned molecules can be detected for the MA (FA) lattice (see Fig. 7).

In order to gain further insight into the depolarization process, we relate our MC results to what is expected for a simple Arrhenius decay of the macroscopic polarization. In the first approximation the dipole rotational rate k can be

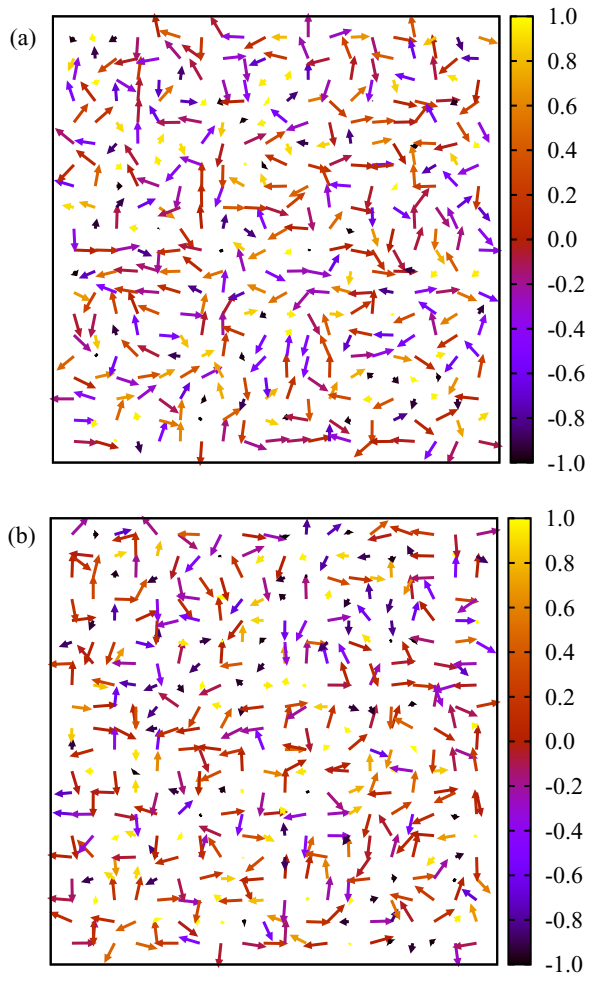

FIG. 7. Dipole distribution over a cross section of the simulation cell after a MC equilibration time of 5×10^5 MC steps for (a) MA and (b) FA. In the picture the angle in the x-y plane is represented by the direction of the arrow, while the one along z is represented by the color code.

described as

$$k = k_0 e^{-N\Delta E/K_B T}, \tag{2}$$

where k_0 is the attempt frequency, ΔE is the activation energy, K_B is Boltzmann's constant, and T is the temperature. Equation (2) describes a process in which N correlated dipoles rotate coherently during the relaxation process. If we insert in the equation the values of k_0 and ΔE provided by the *ab initio* calculations (the attempt frequencies and the barriers for rotation, respectively), we obtain depolarization times in the range of a few picoseconds, in agreement with recent ultrafast two-dimensional vibrational spectroscopy measurements [48]. Furthermore, for completely uncorrelated dipoles, $N = 1$, we find $\tau_{FA}/\tau_{MA} = 5.2$. Such a value slightly overestimates the one obtained with the classical dipole model and the MC simulations. Intriguingly, one can recover the MC results by assuming that in FA and MA the depolarization occurs through the coherent rotation of small dipole clusters of size N. In particular we find that $\tau_{FA}/\tau_{MA} \sim 2$ if $N_{FA} \sim 2$ and $N_{MA} \sim 3$, consistent with the clustering observed in the MC simulations. As such, our relaxation analysis returns to us a situation where the molecule dynamics displays some level of correlation, although a long-range macroscopic order does not emerge.

Finally, we wish to conclude this section by proposing a possible experiment to detect the different molecular relaxations in $MAPbBr_3$ and $FAPbBr_3$ that is able to correlate them to the optical activity of the compounds. In particular we believe that a luminescence decay experiment can fit the scope. The concept here is that, although the molecular electronic energy levels are too far away from the optical gap to play any role, the molecules' orientation affects the shape of the band structure around the gap. This is more visible for $MAPbBr_3$, whose energy gap becomes indirect when the molecules are oriented along the (001) direction. One then expects that the luminescence of hybrid perovskites may depend on the molecule orientation with respect to the crystal axis. In normal conditions the molecules are randomly oriented, so the molecular dynamics is not expected to influence the luminescence decay. However, in a pump-probe configuration one may orient the molecules during the excitation cycle. In that case the different dynamics of the molecule depolarization in $MAPbBr_3$ and $FAPbBr_3$ should translate into different relaxation times.

IV. CONCLUSIONS

In conclusion, by combining DFT calculations including a many-body treatment of the van der Waals interaction and Monte Carlo simulations for a simple dipole model, we have investigated the molecule dynamics in two Br-based hybrid perovskites, namely, $MAPbBr_3$ and $FAPbBr_3$. In general and like for the case of the compounds' I-based counterparts, we have found a relation between the structural and the electronic properties of the compounds, namely, the molecule orientation affects the shape of the conduction and valence bands around the band gap. This means that the dynamics of the molecules may have an effect on the material optical properties. With this in mind we have simulated the depolarization process of both $MAPbBr_3$ and $FAPbBr_3$ and found that the decay constants from a ferroelectric initial condition to a completely depolarized one are different for the two materials. In particular, the ratio between the depolarization times τ_{FA}/τ_{MA} is calculated to be about 2 and is robust against temperature and electric field. We suggest that such findings can possibly be proved in a luminescence decay experiment, which, in principle, can correlate the optical activity with the molecules dynamics.

ACKNOWLEDGMENTS

We acknowledge Dr. P. Docampo for fruitful discussions. We acknowledge Dr. W. Huhn and the FHI-AIMS team for allowing us to use their implementation of SOC prior to publication. This work is sponsored by the European Research Council, QUEST project (C.M. and S.S.), and by the Qatar Environment and Energy Research Institute (F.E.). Computational resources were provided by the supercomputer facilities at the Trinity Center for High Performance Computing and at ICHEC (project tcphy038b and tcphy066b) and by the research computing centre at Texas A&M University at Qatar.

[1] M. A. Green, A. Ho-Baillie, and H. J. Snaith, Nat. Photonics **8**, 506 (2014).
[2] N.-G. Park, J. Phys. Chem. Lett. **4**, 2423 (2013).
[3] G. Hodes and D. Cahen, Nat. Photonics **8**, 87 (2014).
[4] M. Liu, M. B. Johnston, and H. J. Snaith, Nature (London) **501**, 395 (2013).
[5] H.-S. Kim, S. H. Im, and N.-G. Park, J. Phys. Chem. C **118**, 5615 (2014).
[6] Y.-H. Kim, H. Cho, J. H. Heo, T.-S. Kim, N. Myoung, C.-L. Lee, S. H. Im, and T.-W. Lee, Adv. Mater. **27**, 1248 (2015).
[7] Z.-K. Tan *et al.*, Nat. Nanotechnol. **9**, 687 (2014).
[8] L. Gil-Escrig, G. Longo, A. Pertegas, C. Roldan-Carmona, A. Soriano, M. Sessolo, and H. J. Bolink, Chem. Commun. **51**, 569 (2015).
[9] R. L. Z. Hoye, M. R. Chua, K. P. Musselman, G. Li, M.-L. Lai, Z.-K. Tan, N. C. Greenham, J. L. MacManus-Driscoll, R. H. Friend, and D. Credgington, Adv. Mater. **27**, 1414 (2015).
[10] L. Dou, Y. Yang, J. You, Z. Hong, W.-H. Chang, G. Li, and Y. Yang, Nat. Commun. **5**, 5404 (2014).
[11] C. Muthu, S. R. Nagamma, and V. C. Nair, RSC Adv. **4**, 55908 (2014).
[12] J. Luo, J.-H. Im, M. T. Mayer, M. Schreier, M. K. Nazeeruddin, N.-G. Park, S. D. Tilley, H. J. Fan, and M. Grätzel, Science **345**, 1593 (2014).
[13] T. Leijtens, G. E. Eperon, N. K. Noel, S. N. Habisreutinger, A. Petrozza, and H. J. Snaith, Adv. Energy Mater. **5**, 1500963 (2015).
[14] J. H. Heo, D. H. Song, and S. H. Im, Adv. Mater. **26**, 8179 (2014).
[15] S. S. Mali, C. S. Shim, and C. K. Hong, NPG Asia Mater. **7**, e208 (2015).
[16] M. F. Aygler, M. D. Weber, B. M. D. Puscher, D. D. Medina, P. Docampo, and R. D. Costa, J. Phys. Chem. C **119**, 12047 (2015).
[17] F. C. Hanusch *et al.*, J. Phys. Chem. Lett. **5**, 2791 (2014).
[18] W. S. Yang, J. H. Noh, N. J. Jeon, Y. C. Kim, S. Ryu, J. Seo, and S. I. Seok, Science **348**, 1234 (2015).
[19] T. Shi, W.-J. Yin, F. Hong, K. Zhu, and Y. Yan, Appl. Phys. Lett. **106**, 103902 (2015).
[20] H. Kunugita *et al.*, Chem. Lett. **44**, 852 (2015).
[21] J. P. Perdew, K. Burke, and M. Ernzerhof, Phys. Rev. Lett. **77**, 3865 (1996).
[22] V. Blum, R. Gehrke, F. Hanke, P. Havu, V. Havu, X. Ren, K. Reuter, and M. Scheffler, Comput. Phys. Commun. **180**, 2175 (2009).
[23] A. Tkatchenko and M. Scheffler, Phys. Rev. Lett. **102**, 073005 (2009).
[24] A. Tkatchenko, R. A. DiStasio, R. Car, and M. Scheffler, Phys. Rev. Lett. **108**, 236402 (2012).
[25] H. J. Monkhorst and J. D. Pack, Phys. Rev. B **13**, 5188 (1976).
[26] W. H. Press, S. A. Teukolsky, W. T. Vetterling, and B. P. Flannery, *Numerical Recipes*, 3rd ed. (Cambridge University Press, Cambridge, 1997).
[27] W. P. Huhn, M. Scheffler, and V. Blum (unpublished).
[28] A. Togo, F. Oba, and I. Tanaka, Phys. Rev. B **78**, 134106 (2008).
[29] Weinan E, W. Ren, and E. Vanden-Eijnden, J. Chem. Phys. **126**, 164103 (2007).
[30] G. Henkelman, B. P. Uberuaga, and H. Jónsson, J. Chem. Phys. **113**, 9901 (2000).
[31] T. Baikie, N. S. Barrow, Y. Fang, P. J. Keenan, P. R. Slater, R. O. Piltz, M. Gutmann, S. G. Mhaisalkar, and T. J. White, J. Mater. Chem. A **3**, 9298 (2015).
[32] C. Motta, F. El-Mellouhi, S. Kais, N. Tabet, F. Alharbi, and S. Sanvito, Nat. Commun. **6**, 7026 (2015).
[33] A. M. A. Leguy *et al.*, Nat. Commun. **6**, 7124 (2015).
[34] A. Otero-de-la Roza, E. R. Johnson, and V. Luaña, Comput. Phys. Commun. **185**, 1007 (2014).
[35] A. Binek, F. C. Hanusch, P. Docampo, and T. Bein, J. Phys. Chem. Lett. **6**, 1249 (2015).
[36] A. Krukau, O. Vydrov, A. Izmaylov, and G. Scuseria, J. Chem. Phys. **125**, 224106 (2006).
[37] J. Even, L. Pedesseau, J.-M. Jancu, and C. Katan, J. Phys. Chem. Lett. **4**, 2999 (2013).
[38] P. Umari, E. Mosconi, and F. De Angelis, Sci. Rep. **4**, 4467 (2014).
[39] A. Amat, E. Mosconi, E. Ronca, C. Quarti, P. Umari, N. M. K. Nazeeruddi, M. Graetzel, and F. De Angelis, Nano Lett. **14**, 3608 (2014).
[40] J. Even, L. Pedesseau, J.-M. Jancu, and C. Katan, Phys. Status Solidi RRL **8**, 31 (2014).
[41] A. Stroppa, D. Di Sante, P. Barone, M. Bokdam, G. Kresse, C. Franchini, M.-H. Whangbo, and S. Picozzi, Nat. Commun. **5**, 5900 (2014).
[42] F. Zheng, L. Z. Tan, S. Liu, and A. M. Rappe, Nano Lett. **15**, 7794 (2015).
[43] J. M. Frost, K. T. Butler, and A. Walsh, APL Mater. **2**, 081506 (2014).
[44] O. Chubykalo, U. Nowak, R. Smirnov-Rueda, M. A. Wongsam, R. W. Chantrell, and J. M. Gonzalez, Phys. Rev. B **67**, 064422 (2003).
[45] X. Z. Cheng, M. B. A. Jalil, H. K. Lee, and Y. Okabe, Phys. Rev. Lett. **96**, 067208 (2006).
[46] See Supplemental Material at http://link.aps.org/supplemental/10.1103/PhysRevB.93.235412 for animations of the depolarization process.
[47] T. Glaser *et al.*, J. Phys. Chem. Lett. **6**, 2913 (2015).
[48] A. A. Bakulin *et al.*, J. Phys. Chem. Lett. **6**, 3663 (2015).